Multilayer Radiation Solution for Boundary-Layer Flow of Gray Gases

H. S. Lee* and J. A. Menart†
University of Minnesota, Minneapolis, Minnesota 55455
and
A. Fakheri‡
Bradley University, Peoria, Illinois 61625

The multilayer radiation solution technique is applied to the combined radiation-convection problem of a laminar boundary-layer flow of gray absorbing-emitting gases over a flat plate. The developing boundary-layer temperature profiles, boundary-layer thickness, and heat transfer from the plate are presented as functions of the temperature boundary conditions and radiation strength parameter. Radiation is seen to significantly enhance the heat transfer from the plate, and it alters the shape of the temperature profiles as it increases the boundary-layer thickness. The current boundary-layer solutions are in good comparison with the previously published results by Cess. The accuracy of the radiation solution is also separately considered for layers of known temperatures.

Nomenclature

a = absorption coefficient
C_p = specific heat
$E_3(\kappa)$ = third-order exponential integral function
f = dimensionless stream function [Eq. (9)]
k = thermal conductivity
ℓ = ratio defined in Eq. (1)
L_r = reference length [Eq. (8)]
N_r = radiation strength parameter [Eq. (18)]
Nu_x = convection Nusselt number [Eq. (26)]
Pr = Prandtl number, $\mu C_p/k$
q_r = radiative heat flux
Re_x = Reynolds number, $\rho_\infty u_\infty x/\mu_\infty$
T = absolute temperature
u,v = velocity in the x or y direction
x = coordinate along the plate
y = cross-stream coordinate
ϵ = emissivity
η,ξ = similarity variables [Eqs. (6) and (7)]
κ = optical depth
κ_o = overall optical depth
μ = viscosity
ρ = density
Ψ = stream function [Eqs. (4) and (5)]
σ = Stefan-Boltzmann constant

Superscripts

$*$ = nondimensionalized T and q_r
$+,-$ = radiosity directions

Subscripts

m = medium
N = sublayer location
ref = reference value
w = wall
δ = boundary-layer edge
∞ = freestream

Introduction

THE fully developed laminar boundary-layer flow over a flat plate has been extensively studied, partly because its simplicity allows for a careful study of the interactions of a known flowfield with other phenomena. Investigations of radiative heat transfer interactions with a boundary-layer flow of absorbing-emitting gases have been performed using various radiation solution techniques, and Özişik[1] presents a good description of the problem formulation. Transient combustion,[2,3] and the effects of multistep chemical kinetics[4] have also been studied in this flow configuration. There are also investigations that consider the interactions of radiative heat transfer with combustion in boundary-layer flows.[5,6] This work is an attempt to build a basis for coupled radiation and combustion studies by testing the accuracy of the multilayer radiation solution technique[7] for boundary-layer flow of gray absorbing-emitting gases.

The most common method for treating the gas-phase radiation is the one-dimensional, optically thin approximation. Beier et al.[6] treated a sooty boundary-layer diffusion flame with this approximation. Howe[8] and Koh and DeSilva[9] studied high temperature air boundary layers with an additional assumption that the gas only emits radiant energy. Cess[10] uses a perturbation technique in his analysis to analyze regions a short distance from the leading edge of the plate. Later Cess[11] drops the optically thin approximation and looks at the case of linearized radiation (small temperature differences) with relatively weak conduction and strong radiation.

Viskanta and Grosh[12] considered the case of an optically thick boundary layer using the Rosseland approximation. This simplifies the integro-differential energy equation to a differential equation. While an optically thick laminar boundary layer will not be seen in actual practice for a gas flowing over

Presented as Paper 89-0604 at the AIAA 27th Aerospace Sciences Meeting, Reno, NV, Jan. 9-12 1989; received May 15, 1989; revision received July 27, 1989. Copyright © 1989 American Institute of Aeronautics and Astronautics, Inc. All rights reserved.

*Assistant Professor, Department of Mechanical Engineering. Member AIAA
†Graduate Student, Department of Mechanical Engineering.
‡Associate Professor, Department of Mechanical Engineering.

a plate, Viskanta's analysis provides a fully developed radiation-convection solution in this limit.

Yucel et al.[13] employed the P-1 and P-3 approximations for their radiation analysis. Liu and Shih[5] studied a combusting boundary layer without such approximations. Lockwood and Shah[14] proposed the discrete transfer method for handling the gas-phase radiation. This method has recently been extended by Docherty and Fairweather[15] to include the nongray gas effects using the exponential wideband model.

Our objective is to develop an alternative analysis procedure that is simple and well suited for analyzing boundary layers, where one-dimensional radiation can often be assumed. The proposed radiation solution technique is the multilayer technique.[7] This technique was originally developed to obtain scaled radiative heat transfer solutions in scattering layers. The multilayer solution technique has been proven to be a valuable tool for combined mode heat transfer calculations with scattering media.[7,16]

In this paper, the multilayer technique is applied to gray absorbing-emitting gases in a boundary-layer flow over a flat plate. The energy and radiation equations are presented in the following section. A marching finite-difference scheme is described, which solves the energy equation with the radiation treated as a source term. This is followed by considerations of the accuracy of the multilayer technique. Results of the boundary-layer temperature profiles, boundary-layer thickness, and heat transfer from the plate are then presented and discussed.

Analysis

Governing Equations

The steady-state heat transfer solution to the fully developed laminar boundary-layer flow of an ideal, absorbing-emitting gas over a flat plate is addressed. The well-known Prandtl boundary-layer approximations are made in the momentum and energy equations. Body forces in the momentum equation are neglected, and the gas is assumed to have a constant C_p. The gas properties are also assumed to behave in the following manner:

$$\ell = \rho\mu/\rho_\infty\mu_\infty = \text{const} \tag{1}$$

$$Pr = \mu C_p/k = \text{const} \tag{2}$$

$$a/\rho = \text{const} \tag{3}$$

The continuity, momentum, and energy equations for the compressible boundary layer are written with these assumptions[2] and transformed into an incompressible form using the Howarth-Dorodnitzyn transformation.[17] The stream functions are defined as

$$\rho u = \frac{\partial \Psi}{\partial y} \tag{4}$$

$$\rho v = -\frac{\partial \Psi}{\partial x} \tag{5}$$

which satisfy the continuity equation.

The independent coordinates x and y are nondimensionalized as

$$\eta = \left(\frac{u_\infty}{2\rho_\infty\mu_\infty x}\right)^{0.5}\int_0^y \rho\, dy \tag{6}$$

$$\xi = x/L_r \tag{7}$$

where L_r is a reference length chosen to minimize the number of nondimensional parameters in the energy equation and is defined as

$$L_r = \frac{u_\infty}{\rho_\infty\mu_\infty}\frac{\rho^2}{a^2} \tag{8}$$

The nondimensional dependent variables are defined as

$$f = \frac{\Psi}{(2\rho_\infty\mu_\infty u_\infty x)^{0.5}} \tag{9}$$

$$T^* = T/T_w \tag{10}$$

Note that T_w is the reference temperature used throughout this analysis except where specifically noted. Also, $f = f(\eta)$ since the velocity profiles are assumed to be fully developed.

The governing conservation equations written in terms of these nondimensional parameters with the gas property assumptions are

$$\ell\frac{d^3f}{d\eta^3} + f\frac{d^2f}{d\eta^2} = 0 \tag{11}$$

$$\frac{\ell}{Pr}\frac{\partial T^*}{\partial \eta^2} + f\frac{\partial T^*}{\partial \eta} = 2\xi\left(\frac{df}{d\eta}\frac{\partial T^*}{\partial \xi} + \frac{L_r}{\rho u_\infty C_p T_w}\frac{dq_r}{dy}\right) \tag{12}$$

The radiation source term is not expressed in terms of the similarity variable η. Instead, it is nondimensionalized in terms of the optical depth κ as

$$\frac{\partial q_r^*}{\partial \kappa} = \frac{1}{a\sigma T_w^4}\frac{\partial q_r}{\partial y} \tag{13}$$

where

$$q_r^* = \frac{q_r}{\sigma T_w^4} \tag{14}$$

and the optical depth is related to η as

$$\kappa = \int_0^y a\, dy' = \sqrt{2\xi}\eta \tag{15}$$

Substituting Eq. (13) into the energy equation gives

$$\frac{\ell}{Pr}\frac{\partial^2 T^*}{\partial \eta^2} + f\frac{\partial T^*}{\partial \eta} = 2\xi\left(\frac{df}{d\eta}\frac{\partial T^*}{\partial \xi} + N_r\frac{dq_r^*}{d\kappa}\right) \tag{16}$$

where

$$N_r = \frac{L_r\sigma T_w^3}{u_\infty C_p}\frac{a}{\rho} \tag{17}$$

is the radiation strength parameter. When the definition for L_r is substituted from Eq. (8) with the constant gas property assumption of Eq. (3), N_r becomes

$$N_r = \frac{\sigma T_W^3}{\rho_\infty\mu_\infty C_p}\frac{\rho}{a} \tag{18}$$

The effect of the N_r parameter can be compared to the role of Pr in Eq. (16); it gives an indication of the radiation penetration over the momentum diffusion. A larger value signifies a deeper penetration of the radiant energy into the fluid.

The boundary conditions on the transformed momentum equation [Eq. (11)] are

$$f(\eta = 0) = \left.\frac{df}{d\eta}\right|_{\eta=0} = 0 \tag{19a}$$

$$\left.\frac{df}{d\eta}\right|_{\eta\to\infty} = 1.0 \tag{19b}$$

and those for the energy equation are

$$T^*(\eta = 0,\ \xi > 0) = 1.0 \tag{20a}$$

$$T^*(\eta \to \infty,\ \text{all } \xi) = T^*_\infty \tag{20b}$$

$$T^*\ (\text{all } \eta,\ \xi = 0) = T^*_\infty \tag{20c}$$

The multilayer technique is used to obtain the radiation source term $dq_r^*/d\kappa$ in the energy equation. The boundary conditions used in the radiation solution are

$$T^*(\kappa = 0) = 1.0 \tag{21a}$$

$$T^*(\kappa \to \infty) = T^*_\infty \tag{21b}$$

and the diffuse wall emissivity ϵ_w is taken to be one. The freestream boundary condition assumes that the bulk of the fluid in the freestream is large enough that it is similar to a solid wall at T_∞ with $\epsilon_\infty = 1$.

Multilayer Technique

In order to deal with nonisothermal or inhomogeneous layers, a technique for dividing a layer into smaller sublayers was developed. The multilayer solution technique[7] results in sublayers of small thicknesses that are approximately isothermal and homogeneous. The radiative heat flux through such a sublayer can be analyzed with an exact solution, if the input boundary intensity distributions are diffuse. The heat flux distribution for a sublayer, extending from 0 to κ_o, is given by

$$q^*(\kappa) = 2[E_3(\kappa_o - \kappa) - E_3(\kappa)]T_m^{*4} + 2E_3(\kappa)q^{+*}(0) - 2E_3(\kappa_o - \kappa)q^{-*}(\kappa_o) \tag{22}$$

where the nondimensionalization is with respect to σT_{ref}^4, and the nondimensional radiosities $q_r^{+*}(0)$ and $q_r^{-*}(\kappa_o)$ are the incident fluxes at the boundaries.

Energy conservation is obtained by assuming that the heat flux coming out of one layer can be taken to be the diffuse radiosity going into the adjoining layer. Equation (22) can then be written for each sublayer, and the resulting set of linear equations is solved for the positive and negative direction radiosities at every sublayer interface, $q_r^{+*}(\kappa_{N-1})$ and $q_r^{-*}(\kappa_N)$. Once the radiosities are obtained, the heat flux distribution is evaluated with Eq. (22).

Fundamentally the intensity distribution, rather than the directional fluxes, should be conserved at the sublayer interface. Such energy conservation leads to the adding/doubling formulation.[18] By changing the intensity balance to a flux balance, the full matrix manipulations needed for the adding/doubling solution are reduced to a solution of a sparse, five-band matrix for the interface radiosities. Reference 7 shows that the calculations using this technique are accurate to within 10% for isotropically scattering media. The accuracy of the solution for absorbing-emitting layers is discussed in the next section.

The multilayer solution technique is ideal to use in conjunction with a standard finite-difference solution of the energy equation because it divides the calculation domain into many sublayers or control volumes. An initial guess is made on the temperature profile at a given ξ-location. This temperature profile is used to calculate the radiative source term at each η grid point, using Eq. (15) to convert η to κ. The radiative source term, used in the energy equation [Eq. (16)] to get a new temperature profile, is obtained from the multilayer solution. A finite-difference approach is found to be the most accurate way to compute the radiation source term, i.e.,

$$\left(\frac{dq_r^*}{d\kappa}\right)_N = \frac{q_N^* - q_{N-1}^*}{\kappa_N - \kappa_{N-1}} \tag{23}$$

The temperature profiles are updated with the new radiation source term. This iteration process continues until the convergence criterion of less than 0.01% change in T^* is met. This iterative solution process is repeated for the next ξ location by marching downstream. At each ξ-location, the hydrodynamically fully developed dimensionless stream function previously obtained from a numerical solution of the momentum equation [Eq. (11)][2] is used.

Results and Discussion

Accuracy of Multilayer Approximation

In order to get a feel for the accuracy of the multilayer method, it is helpful to look at just the radiative heat transfer results for layers of known temperature distributions. Three simple cases are considered that have exact analytical solutions. The cases shown in Fig. 1 are 1) a hot wall $T^*_{w1} = 1.0$ radiating to a cold medium and cold boundary, where T_{w1} is the reference temperature; 2) a hot medium at $T^*_m = 1.0$ radiating to two cold walls, where T_m is the reference temperature; and 3) a hot wall at $T^*_{w1} = 1.0$ radiating into a medium with the temperatures gradually decreasing to $T^*_{w2} = 0.5$, where T_{w1} is the reference temperature. The medium temperature distribution is given by

$$T^*_m = \left(-\frac{15}{16}\frac{\kappa}{\kappa_o} + 1.0\right)^{0.25} \tag{24}$$

The first case approximates a very thin boundary layer. The second case considers the effects of the emission from an isothermal hot gas. The third case approximates a thick boundary layer with a prescribed temperature distribution. The $T^*_{w2} = 0.5$ boundary condition in this case is the same as the $T^*_\infty = 0.5$ freestream condition used in the boundary-layer results presented later.

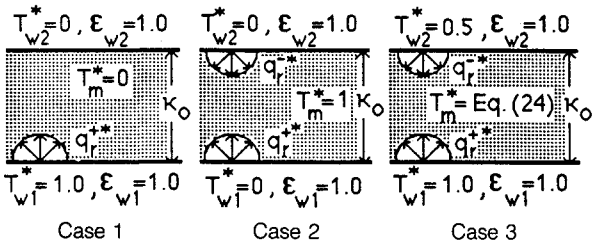

Fig. 1 Simple radiative heat transfer cases.

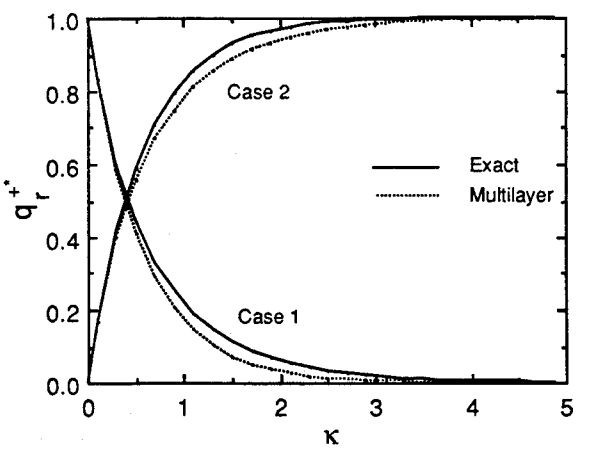

Fig. 2 Radiosity comparisons.

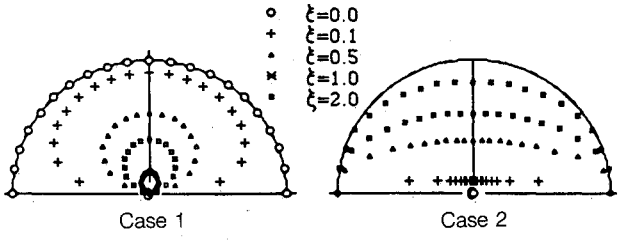

Fig. 3 Intensity distributions.

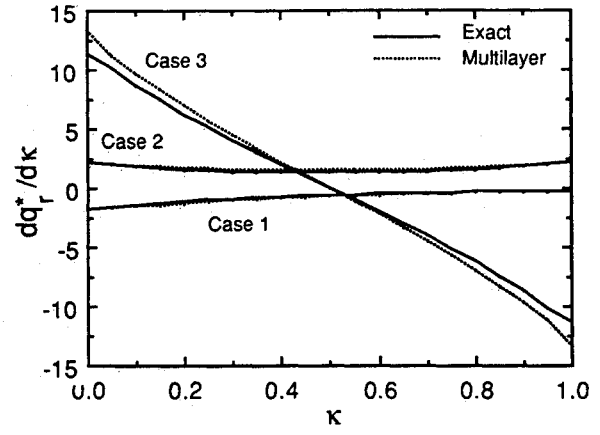

Fig. 4 Radiative source term for $\kappa_o = 1.0$.

Figure 2 shows the exact and the multilayer $q_r^{+*}(\kappa)$ for cases 1 and 2 (σT_{w1}^4 and σT_m^4 are the reference fluxes, respectively). The directional radiosities are the fundamental output by the multilayer technique, and their accuracy is the cornerstone of the method.

For the hot wall radiating into a cold fluid (case 1), $q_r^{+*}(\kappa)$ decreases from one to zero as the radiation travels deeper into the medium. The accuracy of the multilayer solution is excellent for the small optical depths. At large optical depths, the percent differences in the exact and multilayer q_r^{+*} is considerable, but the absolute differences in q_r^{+*} are very small. Maximum differences are seen at optical depths between 0.5 to 3.0, where the multilayer technique underpredicts $q_r^{+*}(\kappa)$. The emitted flux for case 2 increases further into the layer, and the differences between the exact and multilayer q_r^{+*} are also very small, the largest differences occurring at the intermediate optical depths.

The reason for the errors shown in Fig. 2 is that the multilayer technique takes the actual skewed intensity distribution and makes it diffuse at each sublayer interface. Even the intensity emitted from a diffuse wall becomes skewed once it goes through an absorbing layer, and the diffuse approximation becomes worse for case 1 further into the medium. The actual intensity profile for an emitting gas (case 2) gets more diffuse further into the medium. Figure 3 shows the intensity distributions from $\kappa = 0$ to 2.0 for the two cases (κ marked as ξ in the figure), calculated using a one-dimensional S-N discrete ordinates code.[19]

The multilayer technique is intended to supply the radiation source term in the energy equation. Figure 4 presents $dq_r^*/d\kappa$ for $\kappa_o = 1.0$. The multilayer technique's prediction of the radiation source term is very good for the two isothermal cases 1 and 2. The average errors for the nonisothermal case 3 for three different optical depths are 8% for $\kappa_o = 0.1$, 11% for $\kappa_o = 1.0$, and 21% for $\kappa_o = 5.0$. The error percentages are larger when the optical depth is larger, since $dq_r^*/d\kappa$ becomes small. These errors are also found to change for different temperature distributions in the gas layer.

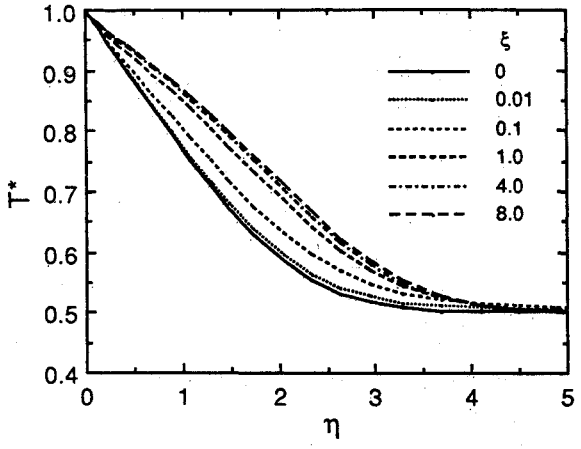

Fig. 5 Temperature profiles for $T_\infty^* = 0.5$, $N_r = 0.1$.

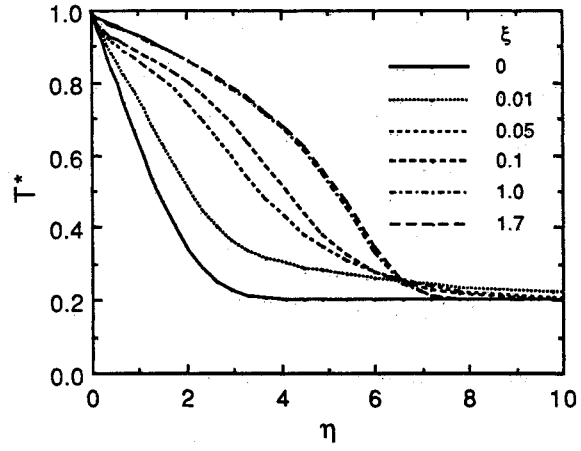

Fig. 6 Temperature profiles for $T_\infty^* = 0.2$, $N_r = 0.1$.

Boundary-Layer Results

The problem of radiative heat transfer combined with conduction and convection in the boundary layer is dependent on five independent parameters. These parameters are T_∞^*, N_r, Pr, ℓ, and ϵ_w. In this analysis, Pr, ℓ, and ϵ_w are taken to be equal to one, although other values can easily be handled. Graphs of the temperature profiles as a function of T_∞^* and the convective and radiative heat transfer results as a function of N_r are presented. The boundary-layer thickness κ_δ is also presented for $T_\infty^* = 0.5$ and $N_r = 0.1$.

The temperature profiles for the boundary conditions $T_w^* = 1.0$ and $T_\infty^* = 0.5$ with $N_r = 0.1$ are shown in Fig. 5. In the figure, $\eta = 0$ is at the plate, and η increases toward the freestream. The profile for $\xi = 0$ is the pure convection-conduction solution. At small values of ξ, the radiative energy passes through the thin boundary layer and is slowly absorbed by the freestream region causing a negligible temperature increase. There is, therefore, no noticeable difference in the temperature distributions up to $\xi = 0.01$. The profile is significantly altered from its convection-conduction shape by radiation further down the plate. Far down the plate Fig. 5 appears to show a fully developed temperature profile, as was predicted by Viskanta and Grosh.[12]

Figure 6 shows the temperature profiles developing as a function of ξ for a larger temperature difference, $T_w^* = 1.0$ and $T_\infty^* = 0.2$. Compared to Fig. 5, a larger temperature difference results in increased temperatures at each ξ-location and a deeper penetration of the thermal boundary layer. The flow appears to become fully developed around $\xi \sim 1.0$ for $T_\infty^* = 0.2$, as compared to $\xi > 8.0$ for $T_\infty^* = 0.5$. The shape of

the fully developed temperature profile is also very different for the $T_\infty^* = 0.2$ case. The flatter temperature distribution near the wall is due to the significant amount of re-emission by the hot fluid there. The gas then cools down rapidly near the freestream.

The differences in the temperature profiles between the $T_\infty^* = 0.5$ and 0.2 were seen for all the N_r values considered: $N_r = 0.1$, 1.0, and 10.0. For both T_∞^* values, the higher temperatures in the boundary layer occur sooner in ξ as N_r increases. The fully developed region also occurs at smaller ξ for the stronger radiation cases of $N_r = 1.0$ and 10.0. There is also a significantly larger penetration of the thermal boundary layer, i.e., the freestream temperature is approached further out in η when N_r is large.

There were some numerical instabilities in what appears to be the fully developed region. This difficulty occurred sooner for the strong radiation and low T_∞^* cases. The instabilities are attributable to a combination of errors as the control volume thickness in terms of κ increases in the downstream direction. There is also discretization error, since the large sublayers cannot be really isothermal. The radiation source term fluctuates around zero at large optical depths. The use of central differencing in the η direction also contributes to the numerical instability.

Radiation is seen to increase the thermal boundary-layer thickness κ_δ in Fig. 7 for $T_\infty^* = 0.5$ and $N_r = 0.1$. The boundary-layer thickness is defined as the optical depth where

$$T_\delta = T_w - 0.99(T_w - T_\infty) \tag{25}$$

Although not presented in the figure, the increase in κ_δ is larger for the $T_\infty^* = 0.2$ case and the stronger radiation cases. When the boundary-layer thickness is presented in terms of the η coordinate, it appears as if the boundary layer expands and then contracts along the plate. The same quantity in terms of κ in Fig. 7 shows that the boundary-layer thickness continually increases downstream.

Results for the convective heat transfer from the plate are given in Fig. 8 for $T_\infty^* = 0.5$. The convective heat transfer is presented in terms of a Nusselt-Reynolds number combination,

$$\frac{Nu_x}{\sqrt{Re_x}} = \frac{I}{\sqrt{2}(T_w^* - T_\infty^*)} \left.\frac{\partial T^*}{\partial \eta}\right|_{\eta=0} \tag{26}$$

which is standard for a pure convection problem. The curves in Fig. 8 cannot be directly interpreted as representing the convective heat transfer from the plate, which does continually decrease as the fluid travels down the plate. The figure does allow for a direct comparison of the combined heat transfer results to that of the pure convection result, $Nu_x/Re_x^{0.5} = 0.332$ for all ξ.

Although the temperature profiles of Figs. 5 and 6, as well as the results of Viskanta and Grosh,[12] point to a fully developed flow of optically thick boundary layers at large ξ, the $Nu_x/Re_x^{0.5}$ curves in Fig. 8 do not become exactly horizontal at far distances down the plate. This is probably because it was not possible to carry the analysis accurately to larger ξ values. The numerical instabilities at large ξ, and the required accuracy in the temperature distribution for convective heat trans-

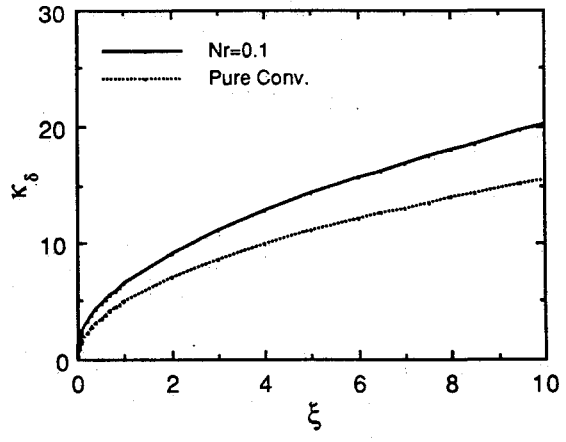

Fig. 7 Thermal boundary-layer thickness for $T_\infty^* = 0.5$.

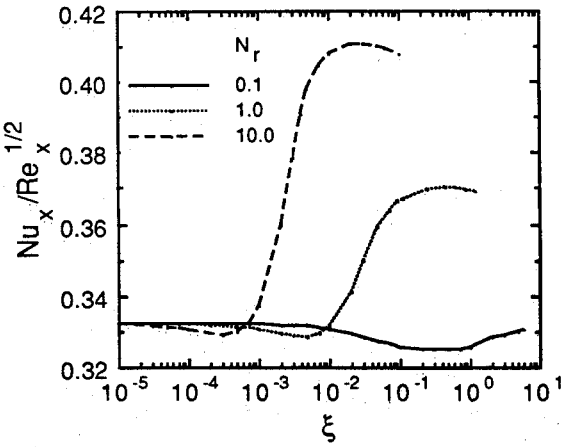

Fig. 8 Convective heat transfer for $T_\infty^* = 0.5$.

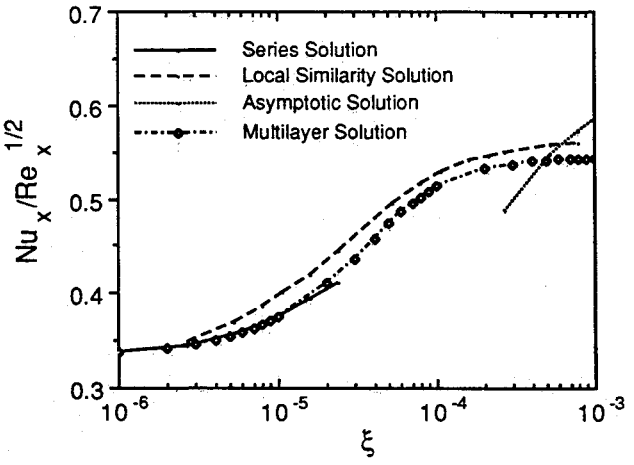

Fig. 9 Convective heat transfer comparison to Cess.[11]

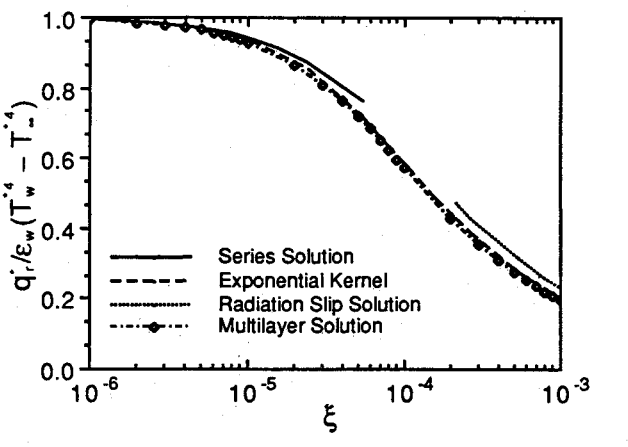

Fig. 10 Radiative heat transfer comparison to Cess.[11]

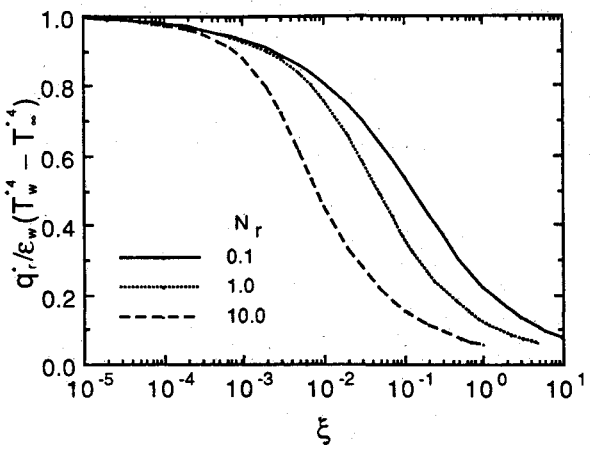

Fig. 11 Radiative heat transfer for $T_\infty^* = 0.5$.

fer calculations, limit the range of a reliable solution domain. Attempting to extend the calculation to larger values of ξ leads to fluctuations in the computed results.

All the curves in Fig. 8 do show a decreasing trend in the small ξ region of the boundary layer as predicted by the optically thin limit solution of Cess.[10] The minimum values in these curves are seen to shift toward the front of the plate as N_r increases. The same is true when T_∞^* decreases, although the minimum is more pronounced for the lower T_∞^* cases.

Cess[11] later presents a more general solution using approximation techniques, one for small ξ (series solution), one for large ξ (asymptotic solution), and one for the region in between (local similarity solution). These three approximate solutions are plotted in Fig. 9 along with the multilayer solution for comparison. Since Cess only considers the limit of linearized radiation and $N_r \to \infty$ in Ref. 11, T_∞^* was taken to be 0.95, and N_r was set equal to 1878 for the multilayer solution. In general, the multilayer solution is close to the local similarity solution, and it shows excellent agreement with the series solution. At large ξ, the multilayer solution is still closer to the local similarity solution than the asymptotic solution.

Figure 10 shows the comparisons of the multilayer wall radiative heat transfer solution and three different approximate solutions by Cess.[11] The radiative part of the heat transfer is presented in the form

$$\frac{q_r^*}{\epsilon_w(T_w^{*4} - T_\infty^{*4})} = \frac{q_r}{\epsilon_w \sigma(T_w^4 - T_\infty^4)} \tag{27}$$

and it decreases from the maximum value at the tip of the plate as the gas next to the plate gets hotter and emits more energy back toward the plate.[10] For the same conditions as in Fig. 9, the multilayer solution in Fig. 10 is in excellent agreement with the exponential kernel solution, and there are only small deviations from the series and radiation slip solutions.

The graph of the decreasing radiative heat transfer is shown in Fig. 11 for different radiation strengths and $T_\infty^* = 0.5$. The radiative flux at the wall decreases faster at smaller ξ with increasing radiation parameter, and all three cases give the same result for radiative flux at the leading edge of the plate. The radiation heat transfer results for the $T_\infty^* = 0.2$ case are similar in shape to the curves in Fig. 11.

Conclusions

The multilayer radiation solution technique is applied to the combined radiation-convection problem of a boundary-layer flow of gray absorbing-emitting gases over a flat plate. The solution method is relatively easy to formulate and is compatible with the finite-difference grids for the energy equation. Although the technique is approximate in nature, it requires a smaller amount of memory than the adding/doubling of the S-N discrete ordinates method.

The accuracy of the multilayer solution for the combined heat transfer problem of laminar flow over a flat plate is good compared to the approximate solutions by Cess.[11] In the limiting case of optically thin boundary layer close to the leading edge, the accuracy of the multilayer solution is very good. When the boundary layer becomes optically thick far downstream of the leading edge, numerical difficulties make it impossible to reach a fully developed solution. The temperature profiles, however, do seem to point to a full development as predicted by Viskanta and Grosh.[12]

Acknowledgments

This work was supported in part by the National Science Foundation Grant NSF/CBT-8451076. Partial support by the Academic Computing Services and Systems is also acknowledged.

References

[1]Özişik, M. N., *Radiative Transfer and Interactions with Conduction and Convection,* Wiley, New York, 1973, pp. 485–539.

[2]Fakheri, A. and Buckius, R. O., "Transient Catalytic Combustion on a Flat Plate," *Combustion and Flame,* Vol. 52, 1983, pp. 169–184.

[3]Fakheri, A. and Buckius, R. O., "Transient Analysis of Heterogeneous and Homogeneous Combustion in Boundary Layer Flow," *Combustion Science and Technology,* Vol. 53, 1987, pp. 259–275.

[4]Fakheri, A., "Homogeneous Combustion of Propane on an Isothermal Flat Plate," American Society of Mechanical Engineers, New York, ASME Paper 87-WA/FACT-1, 1987.

[5]Liu, C. N. and Shih, T. M., "Laminar, Mixed-Convection, Boundary-Layer Nongray-Radiative, Diffusion Flames," *Journal of Heat Transfer,* Vol. 102, Nov. 1980, pp. 724–730.

[6]Beier, R. A., Pagni, P. J., and Okoh, C. I., "Soot and Radiation in Combusting Boundary Layers," *Combustion Science and Technology,* Vol. 39, 1984, pp. 235–262.

[7]Lee, H. and Buckius, R. O., "Combined Mode Heat Transfer Analysis Utilizing Radiation Scaling," *Journal of Heat Transfer,* Vol. 108, Aug. 1986, pp. 626–632.

[8]Howe, T. J., "Radiation Emission Effects of the Equilibrium Boundary Layer in the Stagnation Region," NASA TN D-1031, 1961.

[9]Koh, J. C. Y. and DeSilva, C. N., "Interaction Between Radiation and Convection in the Hypersonic Boundary Layer on a Flat Plate," *ARS Journal,* Vol. 32, 1962, pp. 739–743.

[10]Cess, R. D., "Radiation Effects Upon Boundary-Layer Flow of an Absorbing Gas," *Journal of Heat Transfer,* Vol. 86, Nov. 1964, pp. 469–475.

[11]Cess, R. D., "The Interaction of Thermal Radiation in Boundary Layer Heat Transfer," *Proceedings of the Third International Heat Transfer Conference,* Chicago, IL, Vol. 5, 1966, pp. 154–163.

[12]Viskanta, R. and Grosh, R. J., "Boundary Layer in Thermal Radiation Absorbing and Emitting Media," *International Journal of Heat Mass Transfer,* Vol. 5, 1962, pp. 795–806.

[13]Yucel, A., Kehtarnavaz, H., and Bayazitoglu, Y., "Interaction of Radiation with the Boundary Layer: Nongray Media," American Society of Mechanical Engineers, New York, ASME Paper 83-HT-33, 1983.

[14]Lockwood, F. C. and Shah, N. G., "A New Radiation Solution Method for Incorporation in General Combustion Prediction Procedures," *Eighteenth Symposium (International) on Combustion,* The Combustion Institute, Pittsburgh, PA, 1981, pp. 1405–1414.

[15]Docherty, P. and Fairweather, M., "Predictions of Radiative Transfer from Nonhomogeneous Combustion Products Using the Discrete Transfer Method," *Combustion and Flame,* Vol. 71, 1988, pp. 79–87.

[16]Lee, H., Chikh, S., and Ma, Y., "Full Thermal Development of Radiatively Participating Media in Poiseuille Flow," AIAA Paper 88-2724, 1988.

[17]Trevino, C. and Sen, M., "Transient Ignition in a Flat Plate Boundary Layer," 27th Heat Transfer and Fluid Mechanics Institute, Univ. of Southern California, 1980, pp. 92–107.

[18]Plass, G. N., Kattawar, G. W., and Catchings, F. E., "Matrix Operator Theory of Radiative Transfer, 1: Rayleigh Scattering," *Applied Optics,* Vol. 12, No. 2, Feb. 1973, pp. 314–329.

[19]Kim, T.-K. and Lee, H., "Effect of Anisotropic Scattering on Radiative Heat Transfer in Two-Dimensional Rectangular Enclosures, *International Journal of Heat Mass Transfer,* Vol. 31, No. 8, 1988, pp. 1711–1721.